Characteristics of the Mean Flow Patterns and Structure of Turbulence in Spiral Gas Streams

W. R. SCHOWALTER and H. F. JOHNSTONE

University of Illinois, Urbana, Illinois

Measurements were made of the flow structures in two types of spiral flow fields. The first was a vortex tube in which air entered one end of an 8-in. pipe through an involute entry and left at the opposite end. The second was a conventional cyclone separator in which the same entry was used.

The experimental results show that the mean and turbulent flow structures are not sensitive to changes in the flow rate, but they are greatly affected by the geometry of the system. In the vortex tube the angular velocity is nearly constant at radial distances less than one-half of the radius of the pipe. The flow patterns in the vortex tube and in the cyclone are not symmetrical with the pipe axis. The asymmetry can be explained by postulating a dynamic center line with helical shape. The longitudinal intensity of turbulence increases sharply near the center of the vortex tube. This is caused primarily by the abrupt decrease in mean velocity near the center. The radial intensity also increases near the center, but near the wall it decreases rapidly with distance from the center. The longitudinal intensity of turbulence in the cyclone is highest near the center and near the wall. The high intensity near the wall is caused both by the decrease in mean velocity and the increase in root-mean-square turbulent velocity.

Spiral flow is used in pulverized coal burners, flash vaporizers, cyclone separators, and other industrial equipment to promote mixing and to separate droplets and particles from gases. A better knowledge of the flow patterns and turbulence profiles in this type of flow should be useful in the design of industrial equipment. In this paper the mean flow patterns and components of the turbulence intensity and velocity products are reported for two types of spiral flow fields.

A diagram of the flow system used is shown in Figure 1. The test section was an 8-in. pipe with the involute entrance shown in Figure 2. In one design the end of the pipe next to the entrance was closed, and the opposite end was open. This will be referred to as a "vortex tube." In the second design the end opposite the entrance was closed, and the exit piece shown in Figure 3 was installed next to the entrance to form a conventional cyclone separator.

At points along the test section 5/16-in. holes were drilled through the pipe for insertion of the instruments used to measure the flow characteristics. The holes that were not in use when the measurements were being made were plugged with modeling clay so that the inside of the pipe had a smooth surface. The location of the holes relative to the entrance is shown in Table 1.

W. R. Schowalter is at Princeton University, Princeton, New Jersey.

MEASURING INSTRUMENTS

The pressure probe shown in Figure 4 was used with a hot-wire anemometer probe to find the direction of the mean velocity vector at points in the flow field.

A constant-current hot-wire anemometer with a crossed-wire probe was used to measure $\vec{U}$ and the turbulent quantities (*9, 10, 11, 13*). The probe was made of 0.00014 in. tungsten wires supported on nickel-plated embroidery needles. The probe was calibrated in the potential cone of a standard nozzle.

The instruments were placed in the desired position in the test section by means of a traversing mechanism which could be moved in radial and vertical directions by means of a turning screw with small pitch. With this device the probes could be located within ± 0.01 in. of the desired position. A similar device was used in the calibration of the instruments.

COORDINATE SYSTEMS USED TO DESCRIBE FLOW

Three sets of coordinate systems are used to describe the flow field. Their geometry and spatial relationship are shown in Figure 5. One is a set of coordinates fixed with respect to the main axis of the test section and shown in Figures 5*a* and 5*b*. The positive z-direction is towards the end of the pipe opposite the entrance section. The positive ϕ-direction is chosen in such a way that U_ϕ is always positive. The other two sets of coordinates are local systems determined by the direction of $\vec{U}$. As shown in Figure 5*b*, z, r, and ϕ are the axes of the fixed system, and $\vec{U}$ is the direction of the mean velocity vector at a point. Transformation from the fixed axes to the first local system is made by specifying a rotation, θ, about the r-axis which determines the η ξ ζ-axes (Figure 5*c*). A second rotation, ψ, about the ζ-axis determines the x' y' z'-axes. (Figure 5d). The x'-axis is in the direction of $\vec{U}$. The ξ-axis is coincident with the r-axis, and the ζ-axis is coincident with the z'-axis.

EXPERIMENTAL PROCEDURE

Measurements were made when the temperature and mean velocity of the air stream were constant. The angle θ was

TABLE 1. LOCATION OF TEST STATIONS IN RELATION TO ENTRANCE

Station	Axial distance from upstream edge of inlet farthest from test station, in.
1	6.9
2	9.4
3	11.9
4	12.9
5	14.9
6	15.9
7	16.9
8	18.9
9	19.9
10	20.9
11	21.9
12	22.9
13	23.9
14	24.9
15	25.9
16	26.9
17	27.9
18	29.0
19	31.4
20	32.4
21	33.4
22	36.5
23	38.5

found from the position of the pressure probe when there was no differential on an inclined manometer connected across the pressure probe taps. For measuring the mean velocity and turbulence quantities the calibrated wires were placed at the desired position at the angle θ. In this way the axes of the wires were in the same plane as the vector $\vec{U}$. For measurements near the wall adjacent to the traversing mechanism the procedure was changed so that only a portion of the hot-wire assembly was inside of the duct and the intersection of the cross wires could be placed in a horizontal plane containing the pipe axis (*13*).

The compensation necessary for each wire was determined by the method described by Kunstman (*9*). The wire temperatures were predetermined so that the compensator settings for the two wires were nearly the same. Then the resistances of the wires at the air temperature were measured, the wires were heated to their respective temperatures, and measurements of the mean current and voltage for each wire were made. After this measurements of $\overline{e_1^2}$, $\overline{e_2^2}$, $\overline{(-e_1 - e_2)^2}$, and $\overline{(-e_1 + e_2)^2}$ were made. The relation of these measurements to flow structure is explained in the Appendix.* Temperature and velocity of the air entering the test section were also recorded.

The mean flow patterns in the vortex tube and in the cyclone were found from the velocity vector $\vec{U}$ measured at different points in the flow field. The velocity of the air entering the vortex tube was 100 ft./sec., while that entering the cyclone was approximately 86 ft./sec. A few measurements were also made at inlet velocities of 62 and 87 ft./sec. in the vortex tube and 42 and 61 ft./sec. in the cyclone. All inlet velocities are average velocities based on the 2-x 4-in. rectangular entry. The turbulent intensities u'_η and u'_r, and the product $\frac{\overline{u_\eta u_r}}{U^2}$ were also measured.

The influence of the pressure probe on the angle θ was investigated by changing the shape of the probe rod. The effect was less than $\pm$ 1 deg. The effect of radial velocity on the measurements with the probe was less than $\pm$ 1 deg.

Similar tests were made to estimate the effect of the hot-wire probe rod on the measurements of $\vec{U}$ and the turbulent quantities. The errors in U and ψ were negligible, but there was a small but significant effect on turbulence measurements. The error is believed to be no greater than 10%.

The validity of the wire response equations derived in the Appendix was checked by making measurements in the manner described above, calculating ψ, rotating the hot-wire probe by this angle, and repeating the measurements to see if ψ, as calculated in the new probe position, was zero. In only one case was the error in ψ larger than 2 deg., and in most cases it was approximately 1 deg. The longitudinal and radial intensities of turbulence (u'_η and u'_r, respectively) which were calculated from data obtained before the probe was rotated agreed within about 10% of the values found when the probe was not rotated. The measured values of the velocity products, such as $\frac{\overline{u_r u_\eta}}{U^2}$, were highly sensitive to errors in ψ, and errors as little as 2 deg. in this quantity caused appreciable errors in the turbulent velocity products (*9*). However the consistency of the trends shown by the products indicates that the relative values were significant. Tests showed that the small degree of roughness caused by the holes in the pipe wall did not affect the results significantly.

MEAN FLOW PATTERN

Figures 6 and 7 show the flow pattern of the lines of constant pitch angle, $\delta = (90 - |\theta|)$. Negative distances from the center line denote positions on the side of the pipe axis opposite the side on which the entry is located and toward the side containing the traversing mechanism. The pitch angle is not sensitive to changes in the inlet velocity. This agrees with the results of Eckert and Hartnett (*2*). The pronounced asymmetry of the flow field is especially evident in the vortex tube. Asymmetrical spiral flow fields have also been reported by Iinoya (*6*). Figure 6 shows that the flow near the wall is a spiral leading away from the entry section at a pitch angle that varies in a quasiperiodic manner but which increases slightly with increasing distance from the entrance. The undulations in the lines of constant pitch angle are present to a lesser degree in the cyclone, as shown in Figure 7.

Profiles of the tangential and axial velocity components in the vortex tube are shown in Figures 8 and 9. No data were taken within about 1 in. of the center line because of the relatively high disturbance of the flow caused by the probes in this region (*2*). Instead of flow with constant angular momentum expected in a true vortex the flow in the central portion of the vortex tube is one of nearly constant angular velocity as shown in Figure 8; that is the eddy viscosity appears to be high in this region. The velocity profile appears to be a result of a combination of this effect and the requirement of zero rotation at the wall. The shapes of the tangential velocity curves are similar to those given by Eckert and Hartnett, who worked at inlet velocities

* Appendix has been deposited as document 6426 with the American Documentation Institute, Photoduplication Service, Library of Congress, Washington 25, D. C., and may be obtained for $1.25 for photoprints or 35 mm microfilm.

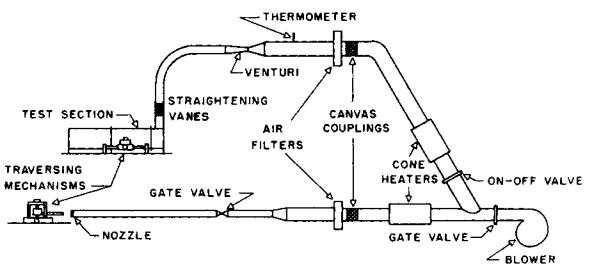

Fig. 1. Schematic diagram of the flow system.

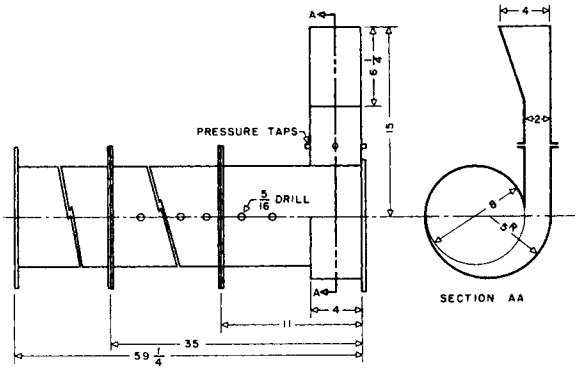

Fig. 2. Test section.

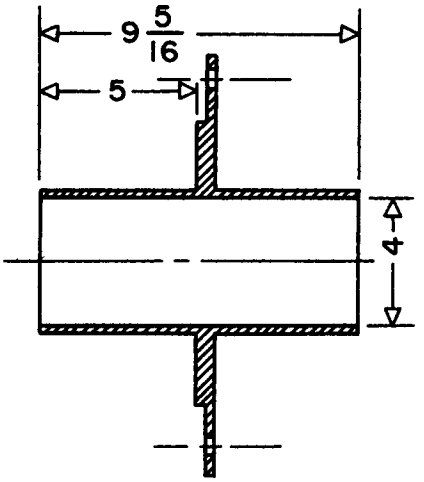

Fig. 3. End fitting for cyclone.

near 500 ft./sec. The similarity is additional evidence of the insensitivity of the flow pattern to changes in the inlet velocity.

Figure 9 shows that the downstream axial flow takes place principally in a zone near the pipe wall. The width of this zone increases with distance from the inlet.

The secondary flow in the vortex tube is shown in Figure 10. The arrows indicate the direction of the velocity vector compounded from the axial and radial velocity components (*13*). Secondary flow exists in any curved bounded flow. In a curved pipe inward flow takes place near the pipe wall because the velocity in this region is lower than that near the axis and the fluid is not being acted upon by a centrifugal force which is equal to the force caused by the surrounding centripetal pressure gradient. The secondary flow in the vortex tube and in the cyclone is caused, at least in part, by a similar action at the boundaries of the flow. Consequently one would expect the geometry of the system to have a pronounced effect on the secondary flow pattern. This may explain the marked difference between the secondary flow pattern obtained in the cyclone, as shown in Figure 11, and that obtained in the vortex tube. It should be noted that the secondary flow pattern in the cyclone is quite different from the symmetrical profiles reported by van Tongeren (*19*) and ter Linden (*17*). The fact that the cyclone used in the present work did not have a conical base may account to some extent for the different secondary flow pattern. It is also possible that the results of van Tongeren and ter Linden are based on data obtained on only one side of the cyclone axis.

The asymmetry of the results indicates that the axis of rotation of the fluid is not on the center line of the pipe; rather it is on a curved line which follows the undulations in the lines of constant pitch angle and moves from one side of the z-axis to the other. This undulating, or dynamic, center line is shown by the curved center line in Figures 6 and 7. Undoubtedly the true center line is not in a singe plane, but it has the shape of a drawn out helix which makes only a few revolutions throughout the length of the tube. When the values of U_ϕ in Figure 8 which are equidistant from the z-axis and within 2 in. of it are compared for opposite sides of the center line, they are seen to be nearly symmetrical with respect to the dynamic center line. Near the wall a different situation exists. Figure 8 shows that, at a given station, a lower value of U_ϕ near the z-axis is accompanied by a higher velocity near the wall, compared with the velocity on the opposite side of the z-axis. The rate of increase of tangential velocity with radius is greater on the side of the z-axis containing the dynamic center line because the area available for flow on this side is smaller than on the opposite side. This explains the asymmetry in U_ϕ near the wall.

It is interesting to note that the secondary flow pattern shown in Figure 10 can be divided into three different subpatterns and that the planes dividing these are at points where the dynamic center line crosses the fixed center line of Figure 6. It is evident that

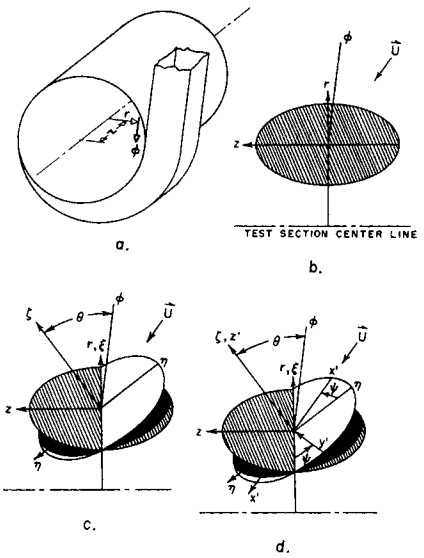

Fig. 5. Transformation of coordinates.

the position of the dynamic center line is related to the secondary flow pattern.

The asymmetry suggests that a spiral flow pattern cannot always be inferred from data obtained on one side of the pipe axis only.

Figures 12 and 13 show the asymmetry in the tangential and axial velocity profiles of the cyclone. Only for a small range of radial distance can the tangential velocity profiles be described accurately by one equation, as proposed by Shepherd and Lapple (*15*) or Broer (*1*). Previous workers (*15, 16, 21*) have described the tangential velocity profiles in cyclones as those of a free vortex, with deviations caused by the viscosity of the fluid. The present profiles show a tendency toward leveling off 2 to 3 in. from the z-axis, or fixed center line. Since it is certain that the tangential velocity decreases rapidly within a distance of about 0.7 in. of the center line (*15, 16*), the tangential velocity profile in the cyclone

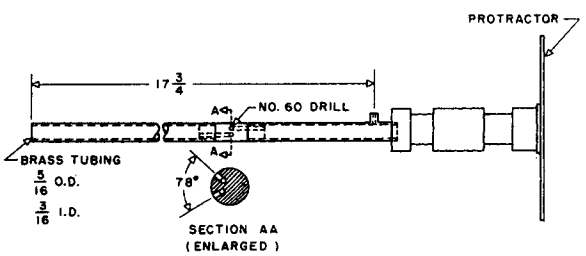

Fig. 4. Pressure probe.

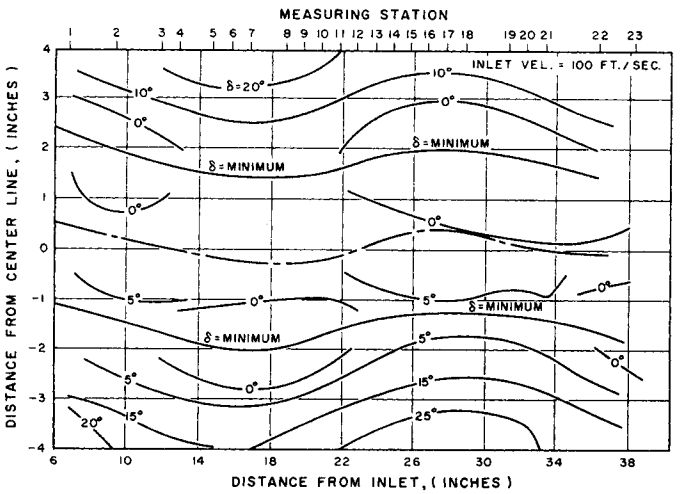

Fig. 6. Lines of constant pitch angle in the vortex tube.

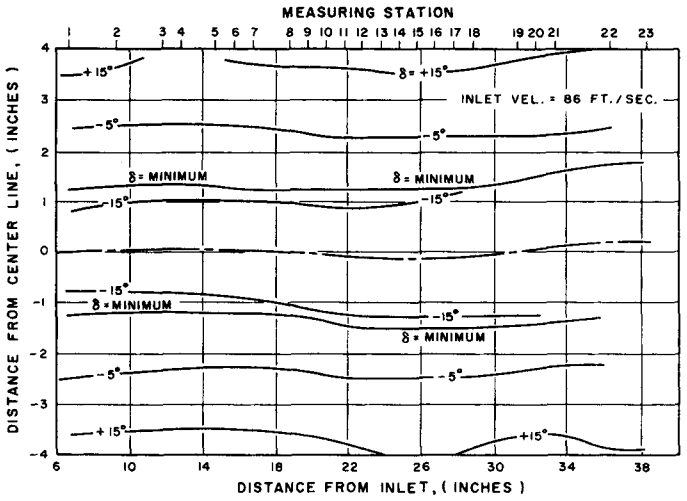

Fig. 7. Lines of constant pitch angle in the cyclone.

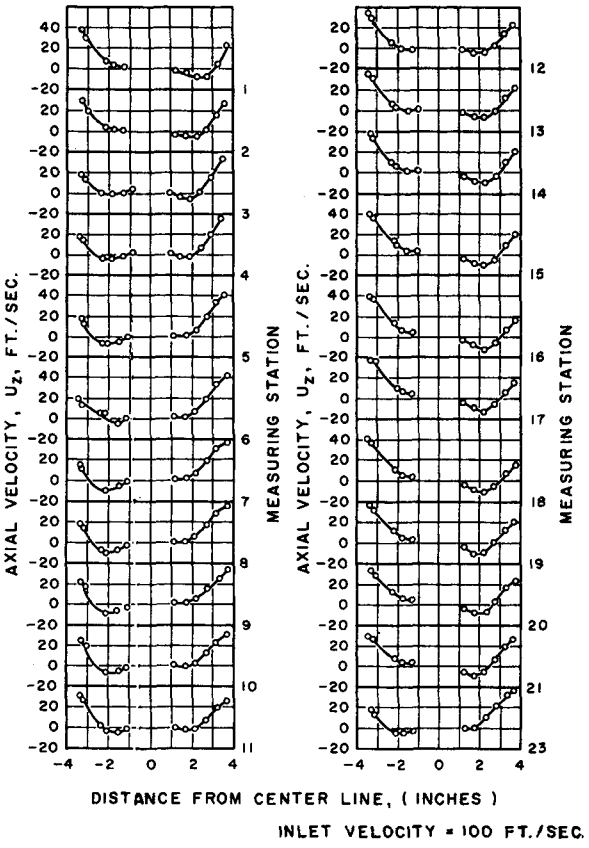

Fig. 9. Axial velocity in the vortex tube.

can be considered to be a superposition of two concentric vortex tube profiles. The profile in the core of the cyclone is similar to that in the vortex tube and the profile in the outer spiral is also similar to that in the vortex tube, but it is prevented from full development by the presence of the inner spiral. This superposition explains the tendency toward a flat tangential velocity profile in the regions from 2 to 3 in. from the z-axis.

Hughes (5) has reported that the method of Einstein and Li (3) may be used to describe the tangential velocity profiles in cyclones. The latter solved the equations of motion for the tangential velocity in a real vortex by assuming that

$$\frac{\partial}{\partial \phi} \cong \frac{\partial}{\partial z} << \frac{\partial}{\partial r}$$

that

$$U_z << U_\phi$$

and that

$$U_r = \frac{-Q_a r}{2\pi r_a^2 l'}, r < r_a \qquad (1)$$

$$U_r = \frac{-Q_a}{2\pi r l'}, r > r_a$$

They also assumed that an eddy viscosity can be defined for a curved flow by the relation

$$\tau_t = \rho \epsilon r \frac{\partial}{\partial r}\left(\frac{U_\phi}{r}\right) \qquad (2)$$

Solutions of the equations of motion are represented by the nondimensional curves shown in Figure 14, where the parameter $A'' = Q_a/2\pi l'(\nu+\epsilon)$. Also shown in Figure 14 are some of the data obtained in the present study and some of the data of Shepherd and Lapple (15). All of the cyclone data are in the range $1 < A'' < 10$. Hughes has reported that reasonable values of ϵ can be obtained for cyclones by using this method, and some of the profiles obtained in the present work also could be used to obtain similar values. This

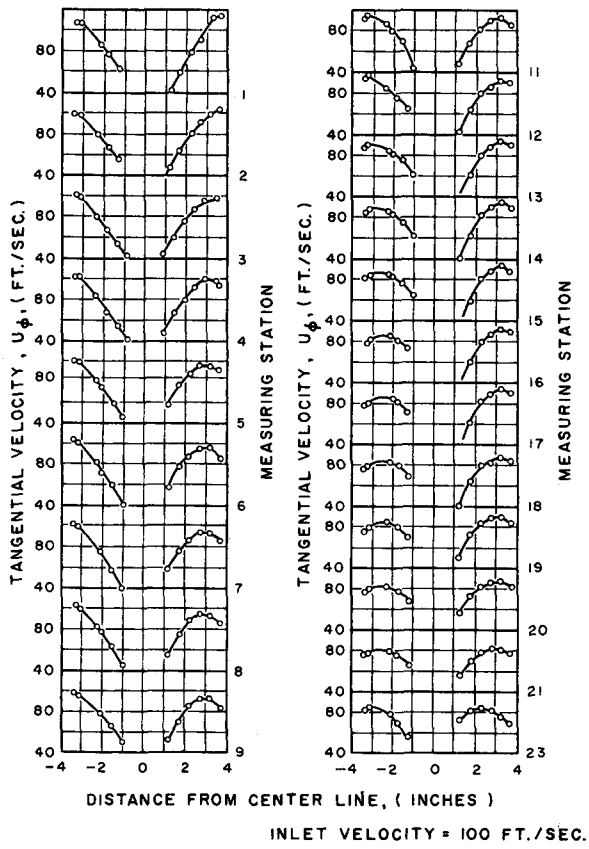

Fig. 8. Tangential velocity in the vortex tube.

agreement however is probably caused fortuitously by cancellation of errors rather than by applicability to cyclone flow fields of the assumptions made in solving the equations of motion. For example Equation (1) does not hold in the vortex tube. Yet reasonable values for ϵ can be obtained from the parameter A'' in Figure 14. The validity of Equation (2) is especially open to question. Various workers (*4, 20*) have shown that the shear stress in two-dimensional curved flow does not vanish at points where $\partial/\partial r(U_\phi/r) = 0$. This is not in agreement with Equation (2).

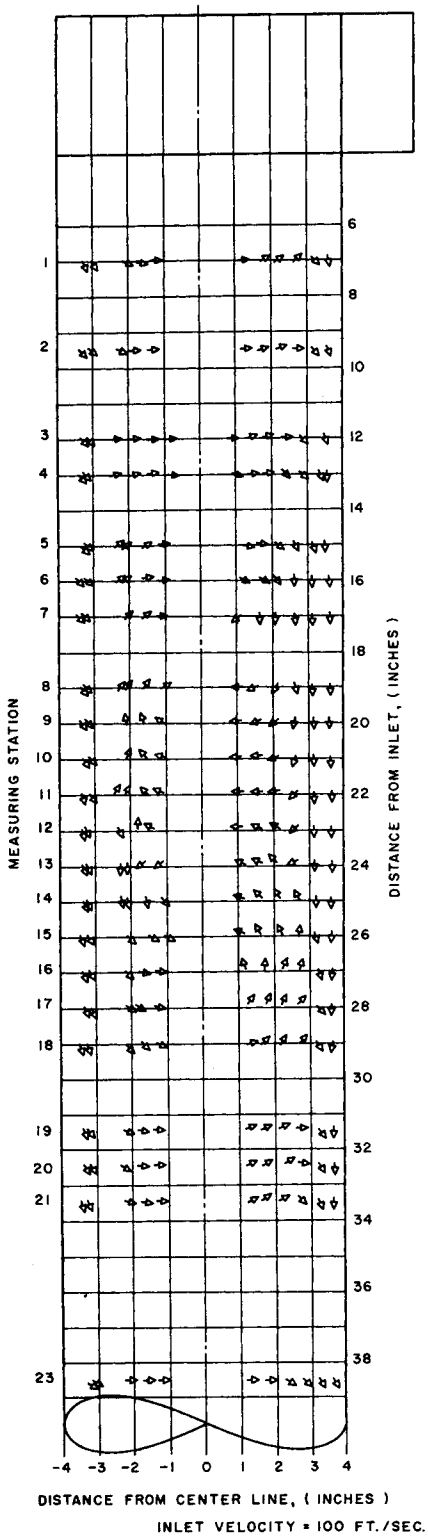

Fig. 10. Secondary flow in the vortex tube.

TURBULENCE MEASUREMENTS

Figure 15 shows that the longitudinal component of turbulent intensity in the vortex tube tends to increase with decreasing distance from the center line. The increase in intensity is caused more by the rapidly decreasing mean velocity than by the intensity in $\sqrt{\overline{u^2_\eta}}$. The intensity profiles are affected by the position of the dynamic center line. For example near the inlet and at points near the z-axis there is a higher intensity on the positive side of the z-axis. This is consistent with the lower mean velocity that exists here for reasons already given.

Eskinazi and Yeh (*4*) have presented the turbulent energy equations

$$\frac{-2U_\phi}{r}\overline{(u_r\,u_\phi)} + \frac{1}{2r}\frac{\partial}{\partial r}\overline{(ru^3_r)} - \frac{\overline{u^2_\phi\,u_r}}{r} = -\frac{1}{\rho}\overline{u_r\frac{\partial p}{\partial r}} + \nu\left[\overline{u_r\,\nabla^2 u_r} - \frac{\overline{u^2_r}}{r^2} - \frac{2}{r^2}\overline{u_r\frac{\partial u_\phi}{\partial \phi}}\right] \quad (3)$$

$$\frac{\overline{u_r\,u_\phi}}{r}\frac{\partial}{\partial r}(rU_\phi) + \frac{1}{2r}\frac{\partial}{\partial r}\overline{(r\,u_r\,u^2_\phi)} + \frac{\overline{u_r\,u^2_\phi}}{r} = -\frac{1}{\rho r}\overline{u_\phi\frac{\partial p}{\partial \phi}} + \nu\left[\overline{u_\phi\,\nabla^2 u_\phi} - \frac{\overline{u^2_\phi}}{r^2} + \frac{2}{r^2}\overline{u_\phi\frac{\partial u_r}{\partial \phi}}\right] \quad (4)$$

for fully developed two-dimensional flow with mean flow in the ϕ-direction only. These conditions are approximated near the wall, and Equations (3) and (4) may be applicable in this region. One other approximation is necessary, since

$$\pm\overline{u_\phi\,u_r} = \overline{u_r\,u_\eta}\sin\theta - \overline{u_r\,u_z}\cos\theta \quad (5)$$

No data are available for $\overline{u_r u_z}$, but in all cases $\sin\theta$ is close to unity and the contribution of the second term is probably not large. The unusual increase in u'_η on the positive side of the center line at Station 1 is in accordance with the relatively large values of $\overline{u_r\,u_\eta}$ which were found here as compared with the values at similar radial distances at other measuring stations. The larger values of $\overline{u_r\,u_\eta}$ give larger negative values for the first term of Equation (4), which is indicative of a greater creation of $\overline{u^2_\phi}$ from the mean flow. A negative sign for the first term of Equations (3) and (4) represents a production of turbulent energy and vice versa. Similarly the low values of $\sqrt{\overline{u^2_\eta}}$ near the wall opposite the entry, that is on the negative side of the center line, are consistent with the change in sign of $\overline{u_r\,u_\eta}$ which was found in this region since the sign of $\partial/\partial r\,(rU_\phi)$ remains constant. The validity of the energy equations is highly questionable in regions where the radial velocity component is appreciable.

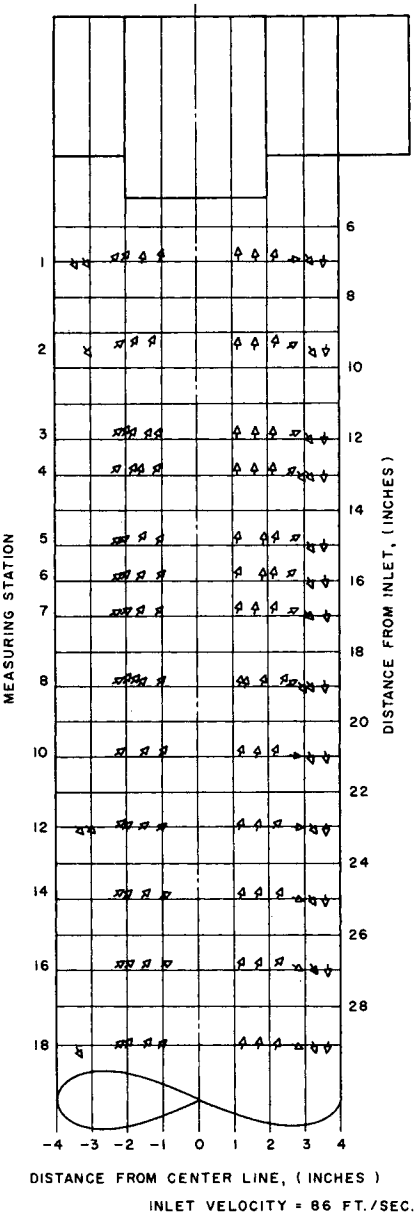

Fig. 11. Secondary flow in the cyclone.

Changes in the sign of $\overline{u_r\,u_\eta}$ were found at points where the angular momentum was not constant with changing radius. This is a common occurrence in curved flows (*4, 20*).

The radial intensity of turbulence in the vortex tube is shown in Figure 16. The suppression of u'_r near the wall agrees with results obtained in other bounded shear flows, such as pipe flow. Again the marked increase of u'_r near

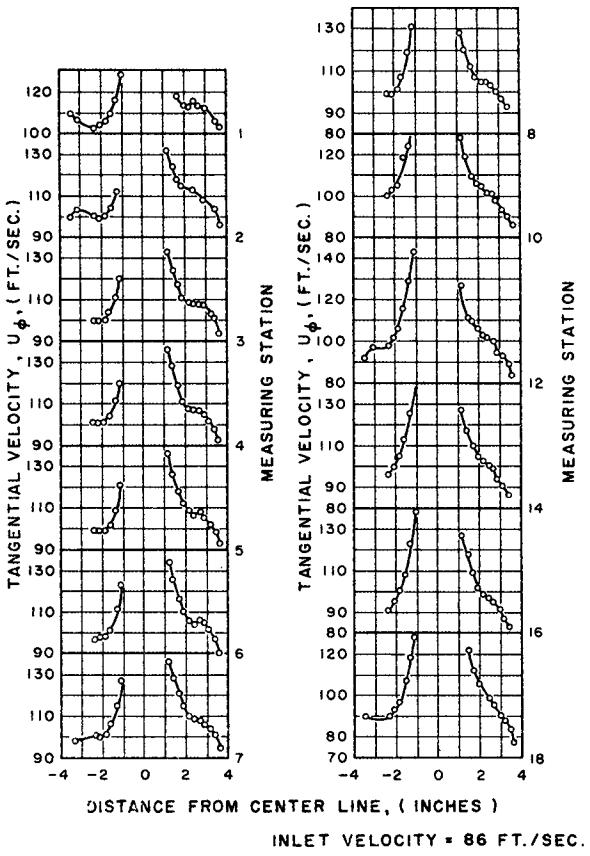

Fig. 12. Tangential velocity in the cyclone.

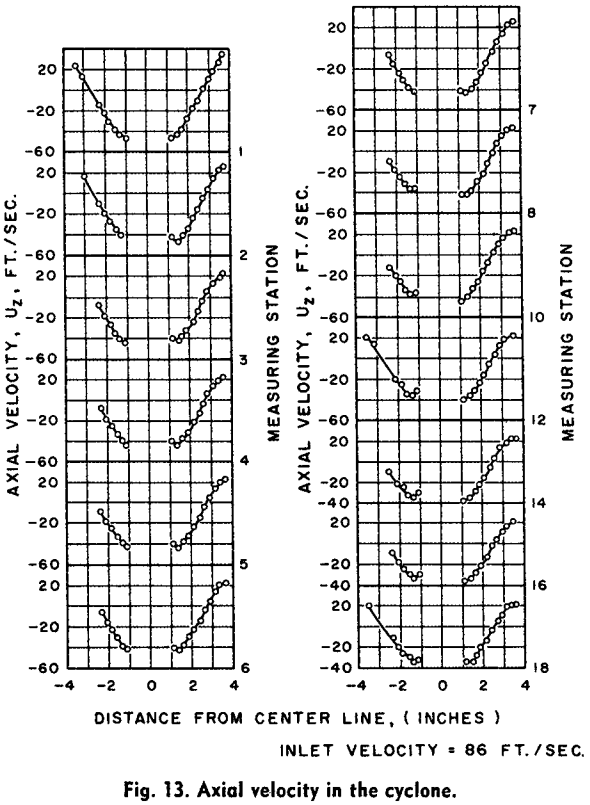

Fig. 13. Axial velocity in the cyclone.

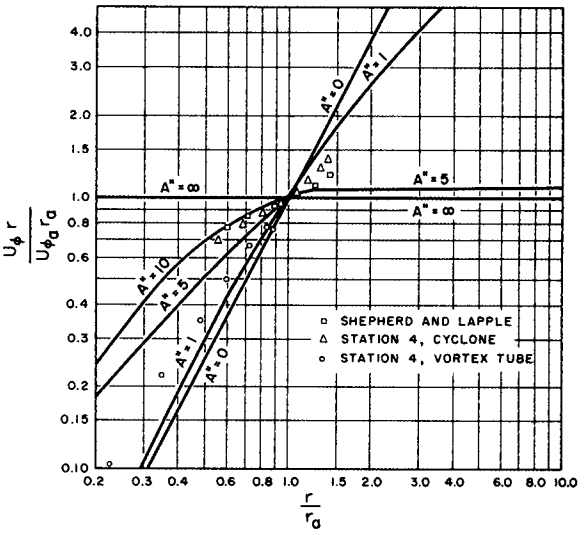

Fig. 14. Tangential velocity profiles compared with equations of Einstein and Li.

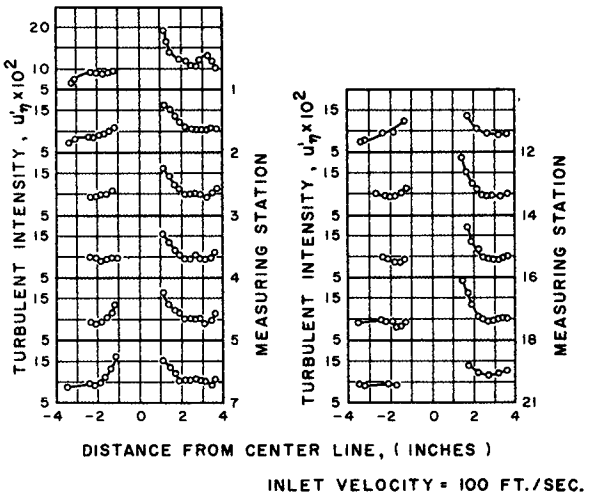

Fig. 15. Longitudinal intensity of turbulence in the vortex tube.

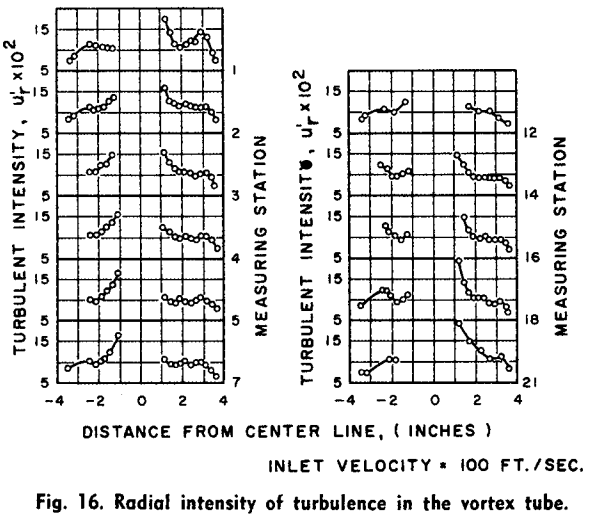

Fig. 16. Radial intensity of turbulence in the vortex tube.

the center is due primarily to the low mean velocity in this region.

Profiles of components of the turbulent intensity in the cyclone are shown in Figures 17 and 18. As before many of the characteristics of these curves can be explained in terms of the mean velocity and the dynamic center line. The fact that u'_η is consistently higher on the positive side of the center line may be caused by the influence of the probe rod on the turbulence.

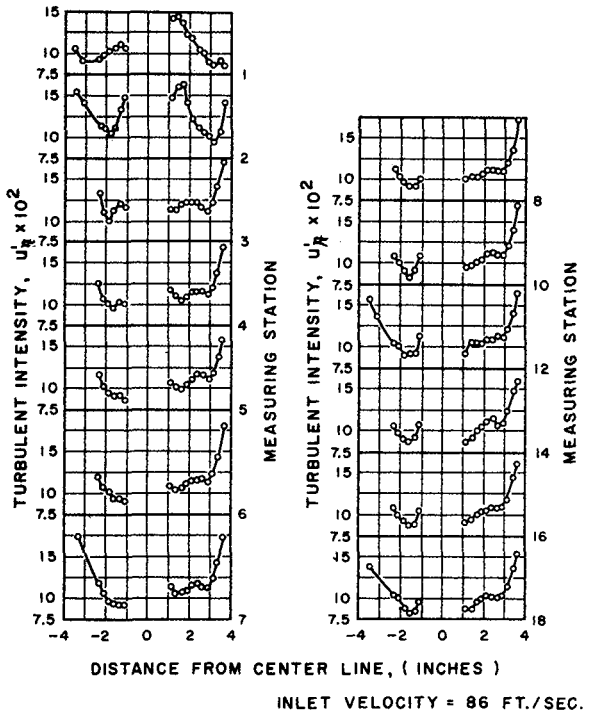

Fig. 17. Longitudinal intensity of turbulence in the cyclone.

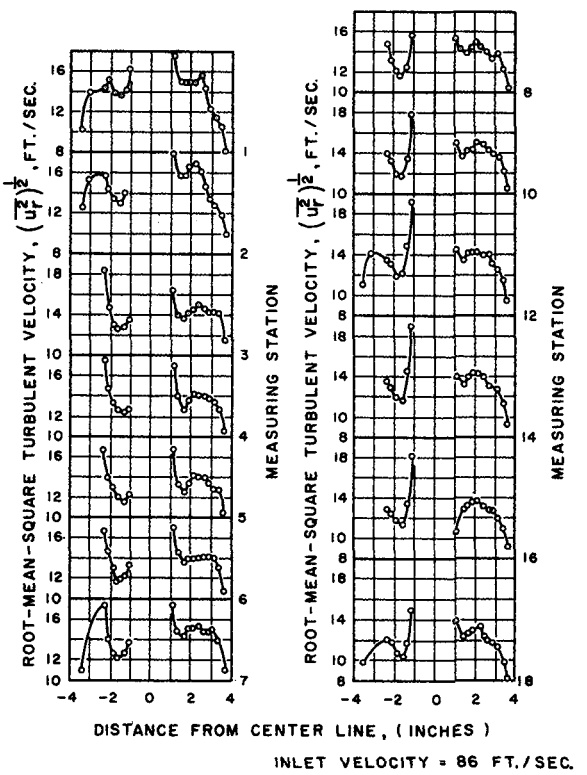

Fig. 19. Root-mean-square radial turbulent velocity in the cyclone.

Figure 19 shows that the asymmetry of the turbulent intensity profiles of u'_r is not caused by changes in U only but that the values of $\sqrt{\overline{u^2_r}}$ are also strongly affected by the distance from the center line. Equation (3) and values of $\overline{u_r u_\eta}$ indicate that the asymmetry in $\sqrt{\overline{u^2_r}}$ near the walls may be caused by the alternate suppression and generation of turbulence from the mean flow.

PRACTICAL CONSEQUENCES OF THE FLOW PATTERNS

Only the radial component of turbulence has an effect on the efficiency of collection of small particles by cyclones. Quantitative calculation of this effect requires a more thorough knowledge of the turbulent structure than is available from this study. However the values of the root mean square fluctuating velocities in the radial direction indicate that the effect of turbulence on separation is likely to be of the same order of magnitude as the effect of secondary flow.

The results also show that the high intensity of turbulence in the central core of a spiral flow field requires that a correction be applied to velocity measurements in this region when these measurements are made with a Pitot tube.

The extreme differences in the flow patterns of the vortex tube and the cyclone indicate one reason why the performance of a Ranque-Hilsch tube is dependent on the fraction of gas leaving at each end (*18*).

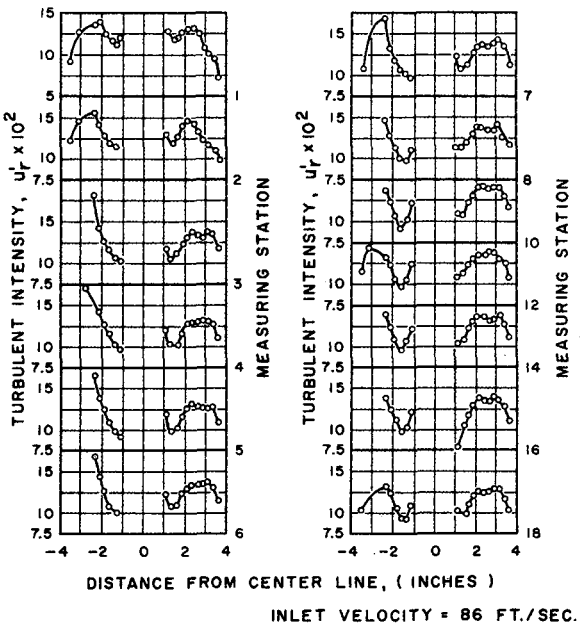

Fig. 18. Radial intensity of turbulence in the cyclone.

CONCLUSIONS

Tangential velocity profiles in the vortex tube show that the angular velocity of the flow is nearly constant at points where $r < 0.5\ r_w$. Tangential velocity profiles in the cyclone can be described by a superposition of two concentric vortex tube profiles.

The flow patterns in both the vortex tube and the cyclone are not symmetrical with the pipe axis. Much of the asymmetry can be explained by postulating a dynamic center line which has the shape of a helix.

The longitudinal intensity of turbulence u'_η increases sharply near the center of the vortex tube. This is caused primarily by the abrupt decrease in mean velocity near the center.

The radial intensity u'_r in the vortex tube shows a similar increase near the center. Near the wall it decreases rapidly with distance from the center, as does u'_r in the cyclone.

In the region studied the longitudinal turbulent intensity u'_η in the cyclone has the highest values near the outer wall. The high intensity near the wall is caused both by the decrease in mean velocity and the increase in $\sqrt{\overline{u^2_\eta}}$.

Some of the phenomena shown by the turbulent intensity profiles near the wall are consistent with a turbulent energy balance based on fully developed two-dimensional curved flow.

The shapes of the profiles of both the mean and turbulent quantities are not significantly affected by flow rate in the range studied.

ACKNOWLEDGMENT

The authors are grateful to E. I. du Pont de Nemours and Company for the support of a fellowship under which this work was accomplished.

NOTATION

A = empirical constant

A'' = $Q_a/2\pi l'(\nu+\epsilon)$

A_d = $$-\frac{\partial H}{\partial(\rho U^0_n)}\cdot\frac{1}{\left(\frac{\partial H}{\partial R_w}\right)-\left(\frac{\partial W}{\partial R_w}\right)}$$

B = empirical constant

C = heat capacity

E_w = mean voltage across wire at T_w

F = $B\sqrt{\sin\beta}$

H = rate of heat loss from wire

I = current

M = time constant of wire

Q_a = volumetric discharge rate through an exit of radius r_a

$R_{a'}$ = wire resistance at some base temperature $T_{a'}$

R_e = wire resistance at T_e

R_w = wire resistance at T_w

$T_{a'}$ = base temperature for computing wire resistance

T_e = temperature of air passing hot wire

T_w = temperature of heated wire

U = magnitude of mean velocity

$\vec{U}$ = mean velocity vector

U_n = mean velocity component normal to wire axis

U_{ϕ_a} = value of U_ϕ at $r = r_a$, neglecting effect of boundary layer

W = electric power supplied to wire and dissipated as heat

e = $e'' + M\,de''/dt$

e'' = fluctuating voltage across wire

l' = length of vortex field from point of discharge

p = fluctuating static pressure

r = distance coordinate in radial direction

r_a = radius of exit tube

t = time

u = fluctuating velocity in the direction of $\vec{U}$

v = fluctuating velocity at right angles to $\vec{U}$ as defined in Figure 5

x' = distance coordinate in the direction of $\vec{U}$

x'' = axis coincident with the axis of the calibration nozzle

y' = distance coordinate defined in Figure 5

z = distance coordinate along axis of test section

z' = distance coordinate defined in Figure 5

Greek Letters

α = thermal coefficient of resistance

β_1 = angle between wire I and x''-axis

β_2 = angle between wire II and x"-axis

γ = $E_w I/(\overline{R_w - R_e})$

δ = pitch angle, = $(90 - |\theta|)$, deg.

δ_1' = $$\frac{F_1\sqrt{U}\,(\overline{R_{w1}-R_e})^2}{2I_1R_e}\cdot\sqrt{\frac{\sin(\beta_1-\psi)}{\sin\beta_1}}$$

δ_2' = $$\frac{F_2\sqrt{U}\,(\overline{R_{w2}-R_e})^2}{2I_2R_e}\cdot\sqrt{\frac{\sin(\beta_2+\psi)}{\sin\beta_2}}$$

ϵ = kinematic eddy viscosity

ζ = distance coordinate defined in Figure 5

η = distance coordinate defined in Figure 5

θ = angle between horizontal plane and a plane containing $\vec{U}$ and the r-axis, defined in Figure 5

ν = kinematic viscosity

ξ = distance coordinate defined in Figure 5

ρ = average density

τ_t = shear stress due to turbulence

ϕ = distance coordinate in the tangential direction with positive direction taken in the direction of $\vec{U}_\phi$

ψ = angle defined in Figure 5

Subscripts

c = value taken during wire calibration

r = component in r-direction

w' = value taken at wall of test section

x' = component in x'-direction

x'' = component in x''-direction

y' = component in y'-direction

z = component in z-direction

z' = component in z'-direction

ζ = component in ζ-direction

η = component in η-direction

ξ = component in ξ-direction

ϕ = component in ϕ-direction

1 = value of wire I

2 = value of wire II

Superscripts

o = instantaneous value

' = when used with a fluctuating quantity it denotes the intensity of that quantity, for example $u'_\phi = \sqrt{\overline{u^2_\phi}}/U$

LITERATURE CITED

1. Broer, L. J. F., *Ingenieur*, **65**, No. 38, 77 (1953).
2. Eckert, E. R. G., and J. P. Hartnett, *Univ. Minn. Heat Transfer Lab. Tech. Rept. No. 6* (1955); "Heat Transfer and Fluid Mechanics Institute," p. 135, Stanford University Press, Stanford, California (1956).
3. Einstein, H. A., and H. Li, *ibid.*, p. 33 (1951).
4. Eskinazi, S., and H. Yeh., *J. Aeronaut. Sci.*, **23**, 23 (1956).
5. Hughes, R. R., *Ind. Eng. Chem.*, **49**, 947 (1957).
6. Iinoya, K., *Mem. Fac. Eng., Nagoya Univ.*, **5**, 131 (1953).
7. King, L. V., *Phil. Trans. Roy. Soc. (London)*, **A214**, 373 (1914).
8. Kovasznay, L. S. G., "High Speed Aerodynamics and Jet Propulsion," vol. IX, pp. 213-283, Princeton Univ. Press, Princeton, New Jersey (1954).
9. Kunstman, R. W., Ph.D. thesis, Univ. Ill., Urbana, Illinois (1952).
10. Romano, J. E., M. S. thesis, Univ. Ill., Urbana, Illinois (1953).
11. ———, Ph.D. thesis, Univ. Ill., Urbana, Illinois (1954).
12. Sandborn, V. A., and J. C. Laurence, *Natl. Advisory Comm. Aeronaut. Tech. Note 3563* (1955).
13. Schowalter, W. R., Ph.D. thesis, Univ. Ill., Urbana, Illinois (1957).
14. Schubauer, G. B., and P. S. Klebanoff, *Natl. Advisory Comm. Aeronaut. Wartime Rept. W86* (1946).
15. Shepherd, C. B., and C. E. Lapple, *Ind. Eng. Chem.*, **31**, 972 (1939).
16. ter Linden, A. J., *Engineering*, **167**, 165 (1949).
17. ———, *Proc. Inst. Mech. Engrs. (London)*, **160**, 233 (1949).
18. van Deemter, J. J., *Appl. Sci. Research*, **A3**, 174 (1952).
19. van Tongeren, H., *Mech. Eng.*, **57**, 753 (1935).
20. Wattendorf, F. L., *Proc. Roy. Soc. (London)*, **A148**, 565 (1935).
21. Yano, T., Y. Kitaura, T. Yamaguchi, and T. Takato, *Chem. Eng. (Japan)*, **19**, 338 (1955).

Manuscript received August 3, 1959; revision received February 17, 1960; paper accepted March 2, 1960. Paper presented at A.I.Ch.E. San Francisco meeting.